# A novel hemispherical spectro-polarimetric scattering instrument for skin lesion imaging

Bruno Boulbry,[*] Thomas A. Germer,[*] and Jessica C. Ramella-Roman[*†]

[*]*Optical Technology Division, National Institute of Standards and Technology, Gaithersburg, MD 20899*
[†]*Department of Biomedical Engineering, The Catholic University of America, Washington, DC 20064*

## ABSTRACT

We present a novel spectro-polarimetric instrument based on hemispherical backscattering for the assessment of superficial skin lesions. The system is capable of capturing polarized light images non-invasively. The effect of the rough skin backscattering is eliminated with the use of out-of-plane illumination. A glass slide with an index matching fluid, commonly used in polarized light imaging, is no longer necessary. The system is composed of sixteen polarized light sources that provide red, green, or blue illumination. The light sources are distributed on a hemispherical shell, and each source produces a collimated beam incident on the center of the hemisphere. A Stokes vector imaging system is mounted on the shell at an oblique angle to the sample normal and consists of a 12-bit scientific camera, two liquid crystal variable retarders, and a fixed polarizer. Stokes vector images of light scattered towards the camera direction are generated for each source. A useful decomposition of the Stokes vector is presented. Examples of images generated by the system are presented.

**Keywords**: imaging, polarization, skin cancer, spectroscopy

## 1. INTRODUCTION

In recent years, several studies have indicated that polarized light could provide noninvasive diagnosis of skin pathologies, such as malignant pigmented and unpigmented skin sites,[1,2] irradiated skin,[3] or mucosa.[4] When a light ray strikes skin, a fraction (a few percent) is reflected by the top surface, while the remainder is propagated into the tissues, where it is either absorbed or scattered by hemoglobin, melanin, or cells. Each of these interactions contributes to a change in polarization state. Polarized light reflected or scattered by the air-tissue interface, for example, can be compared to light scattered by a rough surface and modeled by a facet scattering model.[5,6] Consequently, the top surface contributes mostly to the polarized part of the backscattered light, especially near the specular direction.[6] Light that propagate deeply into the tissue is usually multiply scattered before escaping and is nearly fully depolarized. Light that is weakly scattered by superficial tissues is expected to partially maintain its initial polarization state.[2,7] Therefore, deep subsurface and superficial tissue imaging may be possible using polarization imaging.[2,8–10]

In order to view cancer developing in superficial regions of the skin, a technique using a glass slide contacted on the skin with a drop of water or gel has been developed in order to minimize the effects of the air-tissue interface.[2,5] Additionally deep surface effects were eliminated by only collecting light whose polarization is orthogonal to the incident polarization. Unfortunately, this method may be inappropriate in some cases, such as burn characterization. Furthermore, compression of the skin may alter its optical and physical properties and affect medical diagnosis.[9] Recently, methods to eliminate surface reflection without using flat plates or index-matching fluid have been developed using spectral filtering, combining images obtained from different incident polarization states, and out-of-plane polarized illumination in combination with polarized viewing.[5,9,10]

This proceeding presents a new instrument, which combines these different methods for skin pathology imaging enhancement. Polarized light sources provide illumination in and out of the plane of viewing at three different wavelengths and sixteen different directions. A Stokes vector imaging system is used to detect the light and to separate the polarized component from the unpolarized component and to further decompose the polarized component into two components. Sec. 2 describes the instrument. In Sec. 3, the analysis procedure is presented. A few examples of images obtained with the system are presented in Sec. 4. Finally, the work is summarized in Sec. 5.

Photonic Therapeutics and Diagnostics II, edited by N. Kollias, H. Zeng, B. Choi, R. S. Malek, B. J.-F. Wong, J. F. R. Ilgner, E. A. Trowers, W. T.W. de Riese, H. Hirschberg, S. J. Madsen, M. D. Lucroy, L. P. Tate, K. W. Gregory, G. J. Tearney, Proc. of SPIE Vol. 6078, 60780R, (2006) · 1605-7422/06/$15 · doi: 10.1117/12.648164

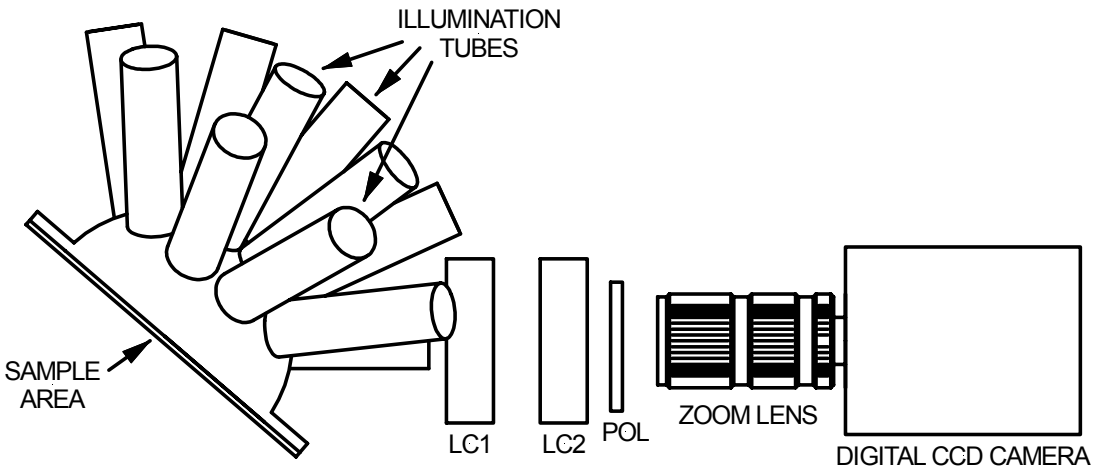


**Figure 1.** Overall schematic of the hemispherical spectro-polarimetric scattering instrument.

## 2. EXPERIMENTAL SET-UP

Figure 1 shows a schematic diagram of the multidirectional-illumination spectro-polarimetric imaging system. It can be divided into two components, a Stokes vector imaging system, which is described in Sec. 2.1, and the illumination system, which is described in Sec. 2.2.

### 2.1. Stokes vector imaging system

A Stokes vector, describing the intensity and polarization state of a beam of light, is given by

$$\mathbf{S} = \begin{pmatrix} S_0 \\ S_1 \\ S_2 \\ S_3 \end{pmatrix} = \begin{pmatrix} I_x + I_y \\ I_x - I_y \\ I_{45°} - I_{-45°} \\ I_{\mathrm{lcp}} - I_{\mathrm{rcp}} \end{pmatrix} \tag{1}$$

where a subscript on the intensity indicates that only that part which is polarized in a particular direction is considered, with lcp and rcp standing for left- and right- circular polarization, respectively. The Stokes vector imaging system consists of two mechanically-fixed liquid crystal variable retarders (LC1 and LC2 in Fig. 1), a fixed thin film polarizer (POL in Fig. 1), a zoom lens, and a 12-bit, 656×496 pixel, digital electron-multiplying charge-coupled device (CCD) camera. The orientations of the liquid crystal retarders, 20° and 135° with respect to the axis of the polarizer, and their respective retardance values, were determined by an optimization method described in Refs. 11 and 12 to maximize the signal-to-noise ratio. Images were obtained for seven different retardance combinations combined for each Stokes vector image. The Stokes vector **S** for each pixel was determined by a matrix multiplication

$$\mathbf{S} = \mathbf{M}\mathbf{I} \tag{2}$$

where **I** is a 7-element vector containing the measured intensities, and **M** is a 4×7 matrix. The matrix **M** is determined by a calibration scheme described in Ref. 13, which does not require precise mechanical positioning of the optical elements in the polarimeter. A separate matrix **M** is required for each operating wavelength. The Stokes vector elements were found to be accurate within 2 % of the intensity element. The integration time of the CCD, held fixed for a specific measurement, was varied between 2 ms and 20 ms, depending upon the sample. A complete set of measurement images, necessary to obtain a Stokes image, requires about 1 s, and is limited by the integration time, the time necessary to switch the states of the liquid crystals, the frame transfer time, and the time necessary to write the images to disk.

### 2.2. Hemispherical tri-color illumination system

The illumination system shown in Figure 1 consists of 16 illumination tubes distributed about a hemisphere. Each illumination tube, illustrated in Fig. 2, contains a tri-color light emitting diode (LED), a thin film polarizer, and a lens. The tri-color LED emits in three bands, red (centered on $\lambda = 642$ nm), green (centered on $\lambda = 521$ nm), or blue (centered on $\lambda = 469$ nm). The widths of the three bands were all about 30 nm, measured full-width at half maximum. Each LED is controlled with a digital and analog input/output module. Each illumination tube produces an approximately collimated beam with a diameter of about 2 cm incident on the sample at the center of the hemisphere. Due to the displacement of the three emitters in each LED module, the beams are somewhat displaced from each other. Furthermore, due to spherical aberration and the non-uniformity of the emitters, the beams are not very uniform at the sample.

Figure 3 shows the orientations of the different illuminators and the camera with respect to the sample normal. Illuminators 1–9 and the camera are centered 49° from the surface normal, illuminators 10–15 are centered 24° from the surface normal, and illuminator 16 is centered on the surface normal. The polarizers in illuminators 5, 10, 13, and 16 are aligned 45° from the plane containing them, while those in the rest of the illuminators are aligned in the plane containing the respective illuminator and the surface normal.

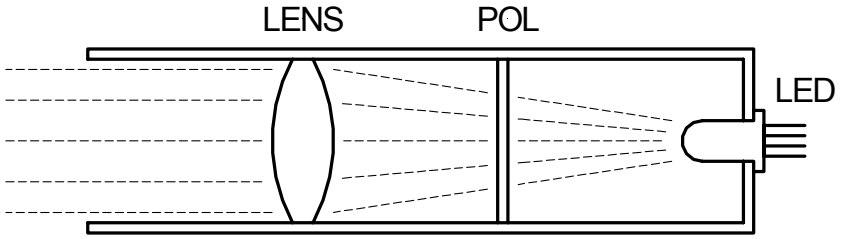


**Figure 2.** Schematic of an illumination tube.

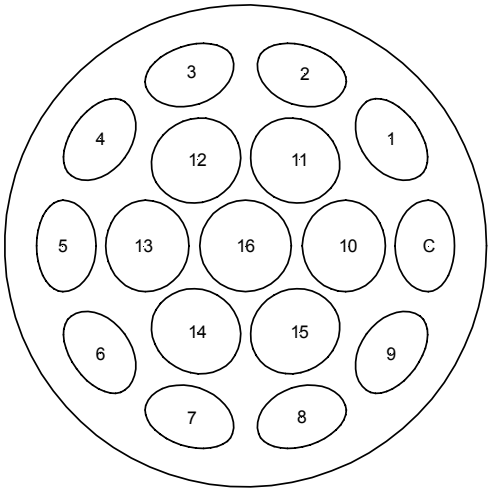


**Figure 3**. The locations of the illuminators (1–16) and the camera (C) with respect to the surface normal.

## 3. ANALYSIS METHOD

The Stokes formalism enables us to express the incoherent superposition of two or more light waves.[14] The Stokes vector **S** of a partially polarized light wave can be decomposed into a completely polarized part $\mathbf{S}_{\text{pol}}$ and a non-polarized part $\mathbf{S}_{\text{unpol}}$. This decomposition is unique:

$$\mathbf{S} = (S_0, S_1, S_2, S_3)^{\mathrm{T}} = \mathbf{S}_{\text{pol}} + \mathbf{S}_{\text{unpol}} = I_{\text{unpol}}(1,0,0,0)^{\mathrm{T}} + I_{\text{pol}}(1, S_1/I_{\text{pol}}, S_2/I_{\text{pol}}, S_3/I_{\text{pol}})^{\mathrm{T}}$$

where

$$I_{\text{unpol}} = S_0 - \sqrt{S_1^{\,2} + S_2^{\,2} + S_3^{\,2}} \tag{3}$$

represents the intensity of the unpolarized part of the light, and

$$I_{\text{pol}} = \sqrt{S_1^{\,2} + S_2^{\,2} + S_3^{\,2}} \tag{4}$$

represents the intensity of the completely polarized part. Given a normalized reference polarization state $\mathbf{S}_{\text{ref}} = (1, s_{\text{ref},1}, s_{\text{ref},2}, s_{\text{ref},3})^{\text{T}}$, the polarized part $\mathbf{S}_{\text{pol}}$ may also be decomposed into the sum of two components,

$$\mathbf{S}_{\text{pol}} = I_{\text{ref}}\mathbf{S}_{\text{ref}} + \bar{I}_{\text{ref}}\bar{\mathbf{S}}_{\text{ref}} \tag{5}$$

where

$$I_{\text{ref}} = \mathbf{S}_{\text{pol}} \cdot \mathbf{S}_{\text{ref}} / 2 \tag{6}$$

represents the intensity of the polarized part, which has the same polarization as the reference,

$$\bar{I}_{\text{ref}} = \mathbf{S}_{\text{pol}} \cdot \bar{\mathbf{S}}_{\text{ref}} / 2 \tag{7}$$

represents the intensity of the polarized part, which is cross-polarized to the reference, and

$$\bar{\mathbf{S}}_{\text{ref}} = (1, -s_{\text{ref},1}, -s_{\text{ref},2}, -s_{\text{ref},3})^{\text{T}}. \tag{8}$$

The usefulness of this decomposition arises from the following arguments. Light which is scattered many times usually becomes highly depolarized. Single scatter sources, on the other hand, often yield distinct polarization states that differ from that observed from different scatter sources. For example, scatter by surface roughness and subsurface features have been shown to yield a small amount of depolarization in certain limits, and they can be distinguished by their polarization states when polarized illumination is used. If our reference polarization $\mathbf{S}_{\text{ref}}$ corresponds to a specific scattering source, say roughness, then $\bar{I}_{\text{ref}}$ will have no contribution from roughness, since it is that part of the total intensity which is cross-polarized with that which could originate from roughness. $\bar{I}_{\text{ref}}$ may represent that part of the scattering which has originated from sources, which do not de-polarize light, but which are not roughness. By using this decomposition, we can possibly separate and distinguish light originating from deep in the tissue, in the superficial tissue, and from the rough interface.

## 4. RESULTS AND DISCUSSION

Measurement were performed on several biological samples, in this paper we show images obtained from an actinic keratosis found on one of the author's skin and a glutaraldehyde phantom introduced beneath porcine skin. The actinic keratosis was encircled with an ink pen. The $\mathbf{S}_{\text{ref}}$ value, Eqs. (5)–(8), was obtained from a piece of ground and partially polished absorbing black glass with an index of refraction of approximately 1.5. For each illumination direction, an average Stokes vector was obtained and used as $\mathbf{S}_{\text{ref}}$ on the respective collected images.

Figure 4 shows the decomposition of an image taken of the actinic keratosis illuminated with blue light from illuminator 14. The normal image and the three components are shown in the figure. The $I_{\text{unpol}}$ image shows little effect of the surface roughness and highlights the actinic keratosis. In contrast, the $I_{\text{ref}}$ image shows little effect of the actinic keratosis, but only the roughness. The $\bar{I}_{\text{ref}}$ image is very dark, suggesting that most of the polarized light is arising from the roughness.

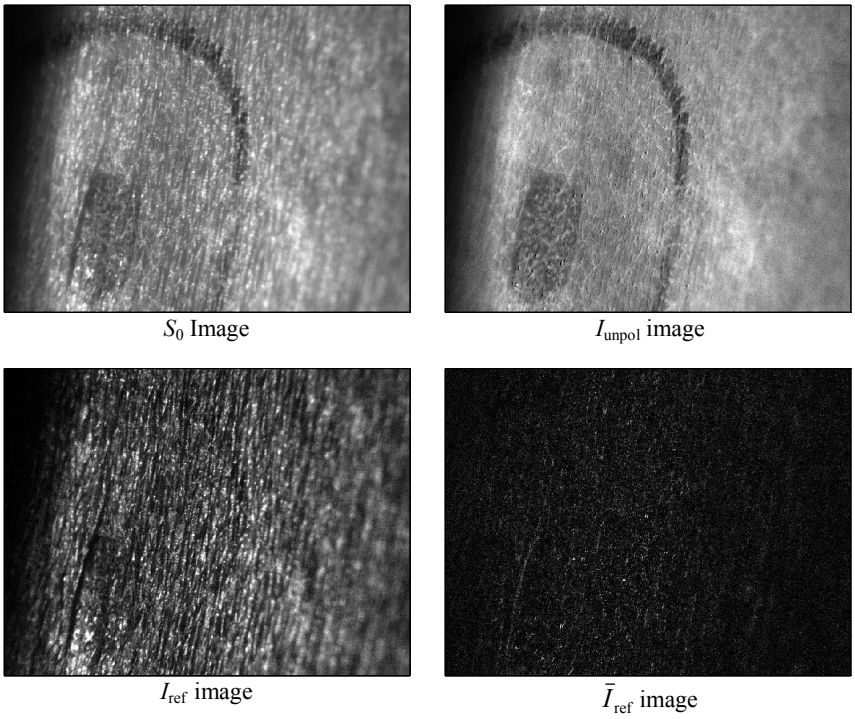


**Figure 4.** Polarization images of an actinic keratosis illuminated with blue light from illuminator 14. The $I_{unpol}$, $I_{ref}$ and $\bar{I}_{ref}$ images are scaled by a factor of 1.5, 2, and 10, respectively, compared to the $S_0$ image.

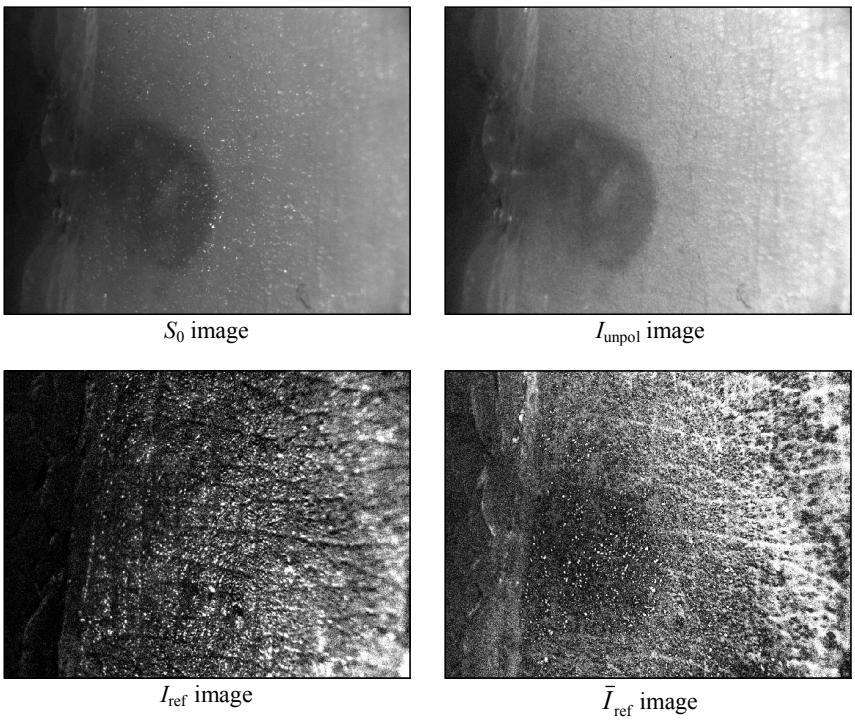


**Figure 5.** Glutaraldehyde phantom in porcine skin illuminated with red light from illuminator 6. The $I_{unpol}$, $I_{ref}$ and $\bar{I}_{ref}$ images are scaled by a factor of 1.5, 20, and 20, respectively, compared to the $S_0$ image.

Figures 5 and 6 show the glutaraldehyde phantom in the porcine skin. Glutaraldehyde (25 % weight fraction in water) was injected from the back of the sample (dermis area) and had the effect of hardening the tissue beneath the skin. Figure 5 shows the phantom illuminated with red light from illuminator 6. One can notice in Fig. 5 that the top rough surface is hardly discernable in the normal ($S_0$) image, and that the $I_{unpol}$ image looks very similar to it, but with less glint. Most of the image results from sub-surface effects. The signal from roughness, $I_{ref}$, shows no discernable effect from the phantom. The $\bar{I}_{ref}$ image shows a small amount of the phantom, while other aspects of the image appear to be a negative of features observed in $I_{ref}$. In this case, the $I_{ref}$ image highlights the roughness.

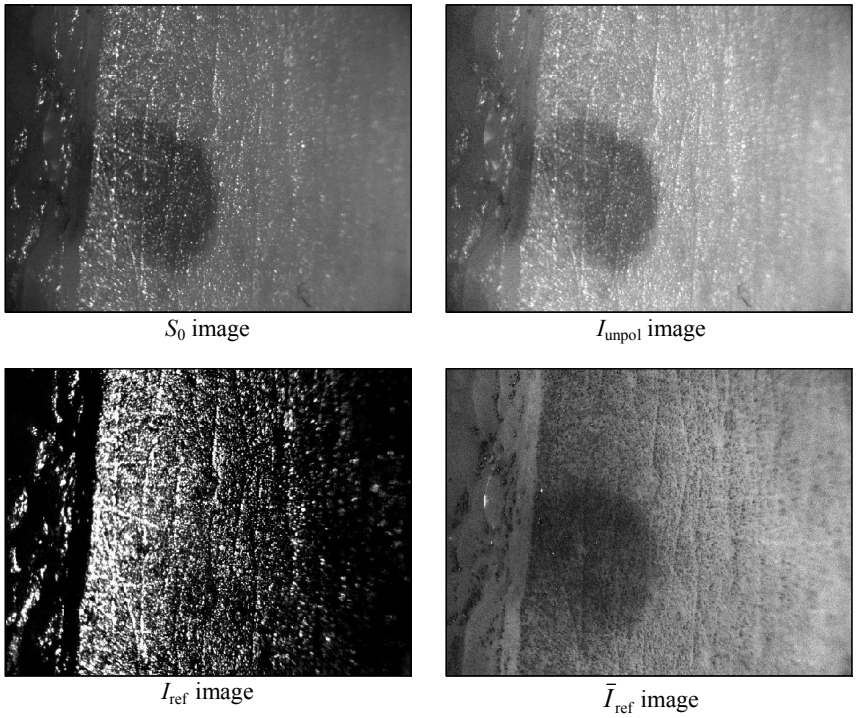


**Figure 6.** Glutaraldehyde phantom in porcine skin illuminated with red light from illuminator 16. The $I_{unpol}$, $I_{ref}$ and $\bar{I}_{ref}$ images are scaled by a factor of 2, 10 and 5, respectively, compared to the $S_0$ image.

Using a different illumination direction, one can observe a different behavior. Figure 6 shows the glutaraldehyde phantom illuminated with red light from illuminator 16. In the $\bar{I}_{ref}$ image, the phantom is much more apparent than it was when it was illuminated with illuminator 6.

One possible improvement upon the method is to not use a reference sample, but instead analyze the statistics of the polarization states observed in the polarized part of the image. Clustering of the polarization state, for example, may reveal multiple scattering sources.[15,16] The reference signal, $\mathbf{S}_{ref}$, can then be chosen to be one of the clustered polarization states. The $I_{ref}$ image and $\bar{I}_{ref}$ image would then allow imaging of two scattering mechanisms.

## 5. CONCLUSIONS AND FUTURE WORK

We have presented a polarized light imaging system and an analysis method to decompose the information that is obtained. Top surface imaging is demonstrated using a reference Stokes vector, and light coming from beneath that surface is detected without using a index-matching contact plate. Subsurface imaging is now conceivable provided that we know the Stokes vector associated with these layers. For this, analysis of the clustering of the Stokes vector on the Poincaré sphere should provide a measure of how many different mechanisms occur in the skin. Trying different sources as reference Stokes vectors would allow us to find the combination (illumination angle and wavelength) which discriminate

these mechanisms the most. We also intend to develop methods that incorporate the signals obtained from all of the different illumination directions.

## REFERENCES


1. M. H. Smith, P. Burke, A. Lompado, E. Tanner, and L. W. Hillman, "Mueller matrix imaging polarimetry in dermatology," Proc. SPIE **3911**, 210-216 (2000).
2. S. L. Jacques, J. C. Ramella-Roman, and K. Lee, "Imaging skin pathology with polarized light," J. Biomed. Opt. **7**, 1-12 (2002).
3. F. Boulvert, B. Boulbry, G. Le Brun, B. Le Jeune, S. Rivet, and J. Cariou, "Analysis of the depolarizing properties of irradiated pig skin," J. Opt. A.: Pure Appl. Opt. **7**, 21-28 (2005).
4. S. G. Demos and R. R. Alfano, "Optical polarization imaging," Appl. Opt. **36**, 150-155 (1997).
5. J. C. Ramella-Roman, D. Duncan, and T. A. Germer, "Out-of-plane polarimetric imaging of skin: Surface and subsurface effects," Proc. SPIE **5686**, 142-153 (2005).
6. T. A. Germer and C. C. Asmail, "Polarization of light scattered by microrough surfaces and subsurface defects," J. Opt. Soc. Am. A **16**, 1326-1332 (1999).
7. V. Sankaran, J. T. Walsh Jr., and D. J. Maitland, "Comparative study of polarized light propagation in biological tissues," J. Biomed. Opt. **7**, 300-306 (2002).
8. S. L. Jacques, M. R. Ostermeyer, L. Wang, and D. Stephens, "Polarized light transmission through skin using video reflectometry: Toward optical tomography of superficial tissue layers," Proc. SPIE **2671**, 199-210 (1996)
9. S. P. Morgan and I. M. Stockford, "Surface-reflection elimination in polarization imaging of superficial tissue," Opt. Lett. **28**, 114-116 (2003).
10. S. G. Demos, H. B. Radousky, and R. R. Alfano, "Deep subsurface imaging in tissues using spectral and polarization filtering," Opt. Express **7**, 23-28 (2000).
11. J. S. Tyo, "Design of optimal polarimeters: maximization of signal-to-noise ratio and minimization of systematic error," Appl. Opt. **41**, 619-630 (2002).
12. D. S. Sabatke, M. R. Descour, E. L. Dereniak, W. C. Sweatt, S. A. Kemme, and G. S. Phipps, "Optimization of retardance for a complete Stokes polarimeter," Opt. Lett. **25**, 802-804 (2000).
13. E. Compain, S. Poirier, and B. Drévillon, "General and self-consistent method for the calibration of polarization modulators, polarimeters, and Mueller-matrix ellipsometers," Appl. Opt. **38**, 3490-3502 (1999).
14. F. Le Roy-Brehonnet and B. Le Jeune, "Utilization of a Mueller matrix formalism to obtain optical targets depolarization and polarization properties," Prog. Quant. Electr. **21**, 109-151 (1997).
15. S. Lakroum, V. Devlaminck, P. Terrier, P. Biela-Enberg, and J. G. Postaire, "Clustering of the Poincaré vectors," IEEE International Conference on Image Processing **2**, 1190-1193 (2005).
16. J. Zallat, C. Collet, and Y. Takakura, "Clustering of polarization-encoded images," Appl. Opt. **2**, 283-292 (2004).